JACS
JOURNAL OF THE AMERICAN CHEMICAL SOCIETY
Article
pubs.acs.org/JACS

Lithium Hexamethyldisilazide-Mediated Enolization of Highly Substituted Aryl Ketones: Structural and Mechanistic Basis of the *E*/*Z* Selectivities

Kyle A. Mack,[‡] Andrew McClory,[†] Haiming Zhang,*[,†] Francis Gosselin,[†] and David B. Collum*[,‡]

[†]Small Molecule Process Chemistry, Genentech, Inc., 1 DNA Way, South San Francisco, California 94080, United States
[‡]Baker Laboratory, Department of Chemistry and Chemical Biology, Cornell University, Ithaca, New York 14853, United States

Supporting Information

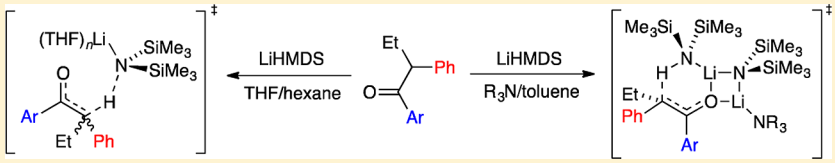

ABSTRACT: Enolizations of highly substituted acyclic ketones used in the syntheses of tetrasubstituted olefin-based anticancer agents are described. Lithium hexamethyldisilazide (LiHMDS)-mediated enolizations are moderately *Z*-selective in neat tetrahydrofuran (THF) and *E*-selective in 2.0 M THF/hexane. The results of NMR spectroscopy show the resulting enolates to be statistically distributed ensembles of *E*,*E*-, *E*,*Z*-, and *Z*,*Z*-enolate dimers with subunits that reflect the selectivities. The results of rate studies trace the preference for *E* and *Z* isomers to tetrasolvated- and pentasolvated-monomer-based transition structures, respectively. Enolization using LiHMDS in *N*,*N*-dimethylethylamine or triethylamine in toluene affords a 65:1 mixture of LiHMDS−lithium enolate mixed dimers containing *E* and *Z* isomers, respectively. Spectroscopic studies show that condition-dependent complexation of ketone to LiHMDS occurs in trialkylamine/toluene. Rate data attribute the high selectivity exclusively to monosolvated-dimer-based transition structures.

INTRODUCTION

As part of our program to develop GDC-0810, a selective estrogen receptor degrader currently in clinical trials for the treatment of breast cancer,[1] we required an efficient and stereoselective synthesis of a tetrasubstituted acyclic all-carbon olefin, a structural motif central to a number of anticancer agents including tamoxifen,[2] idoxifene,[3] and etacstil.[4] Our strategy, outlined in Scheme 1, was fraught with challenges, not the least of which was the requisite *E*-selective enolization en route to desired olefin ***E*-4**.[5]

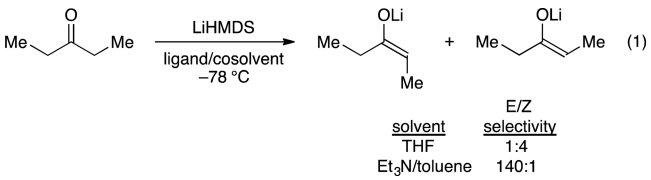

The plan was founded on lithium hexamethyldisilazide (LiHMDS)-mediated enolizations of much simpler ketones showing highly solvent-dependent *E*/*Z* selectivities (eq 1).[6] The dependencies in such uncongested cases derive from markedly different mechanisms corresponding to monomer- and dimer-based transition structures **5** and **6**,[7,8] which offered the possibility that the stereoselectivity would extend to the stereochemically demanding case in Scheme 1. Indeed, 65:1 *E*/*Z* selectivity exceeded expectations.[5] In this paper, we describe the combination of spectroscopic, kinetic, and computational methods used to ascertain the origins of the low selectivities observed with LiHMDS/tetrahydrofuran (THF) and the high selectivities observed with LiHMDS/trialkylamine/toluene.

Scheme 1. Strategy for the Stereoselective Synthesis of Tetrasubstituted Acyclic All-Carbon Olefins

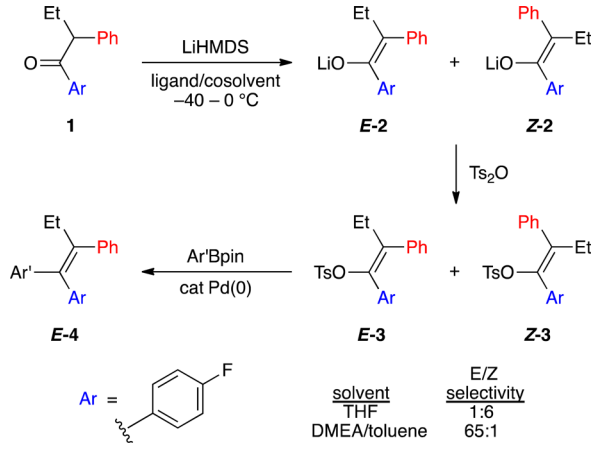

Received: May 16, 2017
Published: August 8, 2017

DOI: 10.1021/jacs.7b05057
J. Am. Chem. Soc. 2017, 139, 12182−12189

5 6

RESULTS

General. LiHMDS, [^{6}Li]LiHMDS, and [^{6}Li, ^{15}N]LiHMDS were prepared and purified as white crystalline solids.[9] Previous studies of LiHMDS described solvent-dependent dimer−monomer mixtures (eq 2), although the equilibrium

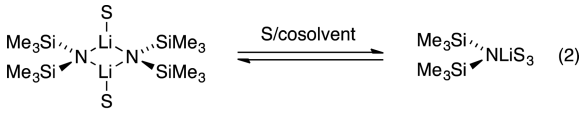

7 8 (2)

was surprisingly sensitive to the choice of hydrocarbon cosolvent (*vide infra*).[10,11] Rate studies were undertaken using the tactics described in two reviews.[12] Density functional theory (DFT) computations were carried out at the B3LYP/6-31G(d) level of theory[13] with single-point MP2 calculations.

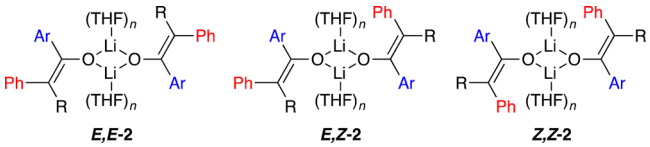

Enolate Structures: THF. The enolization of **1** using [^{6}Li, ^{15}N]LiHMDS in neat THF at 0 °C afforded an ensemble of three resonances recorded at −80 °C and designated ***E,E*-2**, ***E,Z*-2**, and ***Z,Z*-2** (1:32:67; Figure 1A). This result was consistent

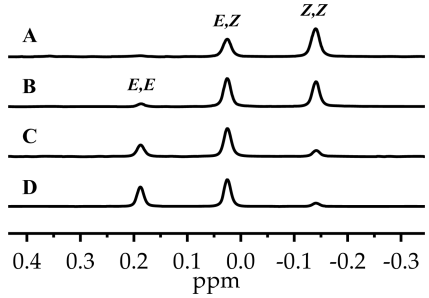

Figure 1. ^{6}Li NMR spectra of mixtures containing ***E,E*-2**, ***E,Z*-2**, and ***Z,Z*-2** from 0.10 M [^{6}Li, ^{15}N]LiHMDS (showing no coupling) and 0.10 M **1** in THF/hexane at −80 °C after aging at 0 °C for 48 h: (A) neat THF (12.2 M); (B) 6.0 M THF/hexane; (C) 4.5 M THF/hexane; (D) 3.0 M THF/hexane. The measured mole fractions (χ_E) of ***E*-2** in A−D are 0.17, 0.30, 0.56, and 0.66, respectively.

with the approximate 1:6 *E*/*Z* selectivity shown with tosylation and subsequent high-performance liquid chromatography analysis.[5] The absence of resonances displaying ^{6}Li−^{15}N coupling confirmed that mixed aggregates were not present. As the THF concentration decreased, the distribution of enolates shifted to favor ***E*-2** (Figure 1B−D) with a concurrent shift in the distribution of isomeric trapped tosylates. The method of continuous variation[14] was used to plot the relative populations of ***E,E*-2**, ***E,Z*-2**, and ***Z,Z*-2** versus the measured mole fraction[15] of the ***E*-2** subunit (χ_E) and obtain a Job plot[16] (Figure 2) confirming the dimer assignment.

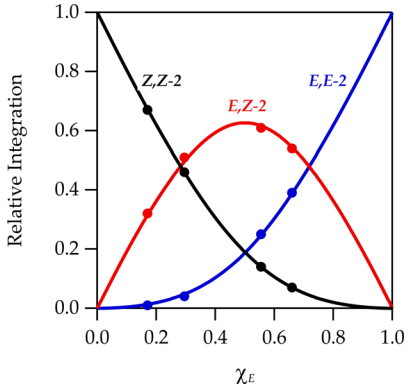

Figure 2. Job plot showing the relative integration of the ^{6}Li resonances versus the measured mole fraction (X_E)[15] of ***E*-2** for 0.10 M mixtures of ***E*-2** and ***Z*-2** at −80 °C and at varying THF concentrations in hexane (see Figure 1).

At <3.0 M THF (the right side of Figure 2), enolate insolubility became a problem. On a positive note, we obtained an X-ray crystal structure that, although of marginal quality, showed a trisolvated tetramer (Figure 3).

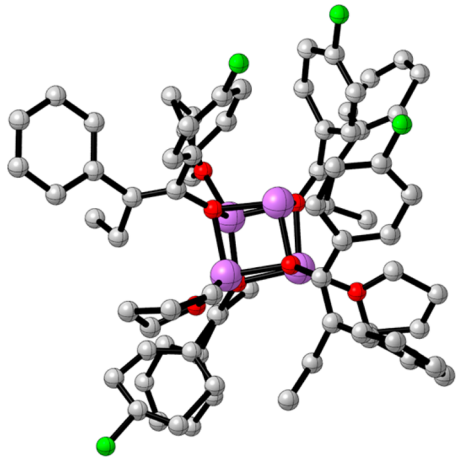

Figure 3. Low-resolution (poor quality) X-ray crystal structure of **2** crystallized from 0.10 M enolate generated in 2.0 M THF/hexane solutions. The compound is a trisolvated tetramer composed of four ***E*-2** subunits.[17]

Computational studies at the B3LYP level of theory with the 6-31G(d) basis set and MP2 correction[13,14] were used to probe some of the inherent properties of the enolate dimers. Serial solvation showed that ***E,E*-2**, ***E,Z*-2**, and ***Z,Z*-2** saturated at tetrasolvation. The heterodimer ***E,Z*-2** showed a small (0.4 kcal/mol) net stabilization, as observed experimentally.

Mechanism of Enolization: THF. Enolizations of **1** (0.010 M) with LiHMDS (0.020−0.20 M) in THF/hexane mixtures (2.0−12.2 M THF) were followed at 0 °C. The results of in situ IR spectroscopy[18] showed that the loss of **1** (1687 cm^{-1}) followed a first-order decay. The pseudo-first-order rate constants (k_{obsd}) were independent of the initial concentration of **1**, consistent with a first-order ketone dependence. Ketone **1** deuterated at the 2-position (**1**-d_1) afforded an isotope effect (k_H/k_D = 6) consistent with rate-limiting proton transfer.

DOI: 10.1021/jacs.7b05057
J. Am. Chem. Soc. 2017, 139, 12182−12189

A plot of initial rates[19] versus THF concentration revealed a deceptively simple dependence; a fit to rate = $a[\mathrm{THF}]^n$ afforded $n = 2.8$ (Figure 4, inset). The deception stemmed from the shift

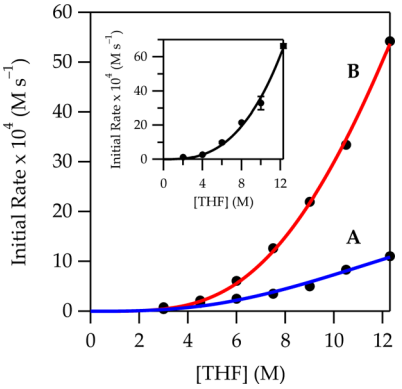

Figure 4. Plot of initial rate vs THF concentration in hexane for the enolization of **1** (0.010 M) with LiHMDS (0.10 M) at 0 °C measured with IR spectroscopy (1687 cm^{-1}). The inset depicts an unweighted least-squares fit to $y = ax^n$ ($a = 0.05 \pm 0.03$, $n = 2.8 \pm 0.2$). Curves A and B represent unweighted least-squares fits to each half of eq 3 (k_1 and k_2, respectively) with $A_2(THF)_2$ described in eq 4. The initial rates for the formation of ***E*-2** were determined by multiplying the proportion of ***E*-2** at a given THF concentration by the total initial rate at that concentration. The initial rates of ***Z*-2** formation were calculated similarly.

of >95% disolvated dimer in 2.0 M THF/hexane to >95% trisolvated monomer in neat THF (eq 2).[10] A simple power function did not account for the dimer−monomer equilibrium or the affiliated change in solvation per Li. If the reaction had proceeded via a single mechanism involving disolvated monomer (AS_2), such as transition structure **5**, a maximum in the plot at intermediate THF concentrations would have been observed.[20] That the rates continue rising even as trisolvated monomer becomes dominant demands that an even more highly solvated form be involved in the enolization. By monitoring the THF-dependent *E*/*Z* selectivities over the analogous range of THF concentrations, we separated the components of the two pathways and showed that they contribute to second- and third-order dependencies (see Figure 4, curves A and B, respectively). Once again, these orders, which are consistent with the measured ratios, were *not* trivial to extract from the data and required fitting to the model discussed below and described in the Supporting Information. Using toluene in place of hexane resulted in no measurable difference in the THF dependence, which seems self-evident except that pronounced hydrocarbon effects on LiHMDS/THF-mediated enolizations have been observed.[20]

A plot of initial rates versus LiHMDS concentration in neat THF, conditions in which trisolvated monomer **8** (eq 2, S = THF) dominated (97%), showed a first-order dependence (Figure 5), confirming that the observable monomer reacts as a monomer. The analogous plot in 2.0 M THF/hexane, which favored dimer (96%), revealed an approximate half-order dependence (Figure 6) consistent with a dimer−monomer pre-equilibrium followed by a monomer-based metalation.

The rate data are consistent with the rate law in eqs 3 and 4 and the mechanism illustrated in eqs 5−7.[21] The complexity stems from solving for $[A_2(THF)_2]$ while accounting for both the shifting ground state—dimer to monomer—and the corresponding change in solvation number per Li. The underlying math is

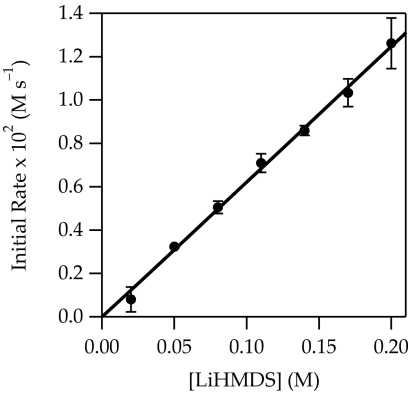

Figure 5. Plot of initial rate vs LiHMDS concentration in neat THF (12.2 M) for the enolization of **1** (0.010 M) at 0 °C measured with IR spectroscopy (1687 cm^{-1}). The curve depicts an unweighted least-squares fit to $y = ax^n$ ($a = 6.3 \pm 0.5$, $n = 1.01 \pm 0.04$).

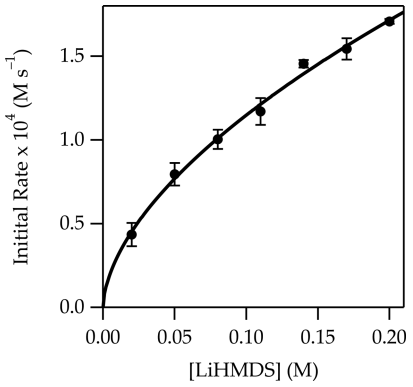

Figure 6. Plot of initial rate vs LiHMDS concentration in 2.0 M THF/hexane for the enolization of **1** (0.010 M) at 0 °C measured with IR spectroscopy (1687 cm^{-1}). The curve depicts an unweighted least-squares fit to $y = ax^n$ ($a = 4.4 \pm 0.2$, $n = 0.58 \pm 0.02$).

beyond the scope of this paper and is relegated to the Supporting Information.

$$\text{Rate} = (k_1[\mathrm{THF}]^3 + k_2[\mathrm{THF}]^4)[\mathbf{1}][A_2(THF)_2]^{1/2} \quad (3)$$

$$[A_2(THF)_2] = \frac{1}{8}(4[A]_0 + K_{eq}[\mathrm{THF}]^4 - \sqrt{K_{eq}}[\mathrm{THF}]^2 \sqrt{8[A]_0 + K_{eq}[\mathrm{THF}]^4}) \quad (4)$$

$$^1/_2 A_2(THF)_2 + 2\mathrm{THF} \overset{K_{eq}}{\rightleftharpoons} A(THF)_3 \quad (5)$$

$$A(THF)_3 + \mathbf{1} \xrightarrow{k_1[\mathrm{THF}]} E \text{ enolate} \quad (6)$$

$$A(THF)_3 + \mathbf{1} \xrightarrow{k_2[\mathrm{THF}]^2} Z \text{ enolate} \quad (7)$$

Structures of LiHMDS/Ketone Complexes: Trialkylamines. The rate studies of LiHMDS/trialkylamine-mediated enolizations were necessarily founded on the structural assignments of LiHMDS in the various trialkylamines with ketone present (Scheme 2). In weakly coordinating trialkylamines, LiHMDS−ketone complexes were readily observed. They differed quantitatively from analogous complexes formed from 2-methylcyclohexanone or 3-pentanone owing to weaker binding.[8]

In the absence of trialkylamines at −100 °C, ketone **1** complexed to LiHMDS dimer **9** to afford mono- and dicomplexed

DOI: 10.1021/jacs.7b05057
J. Am. Chem. Soc. 2017, 139, 12182−12189

Scheme 2. Condition-Dependent Equilibria for LiHMDS/Ketone in DMEA with Toluene Hydrocarbon Cosolvent (−100 °C)

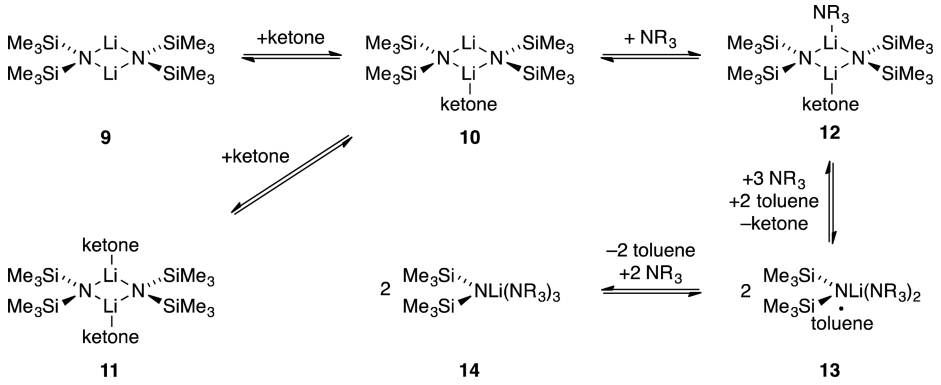

dimers **10** and **11**. Complex **10** displayed an IR absorbance at 1671 cm^{-1} and, in the NMR spectra, two ^{6}Li triplets (1:1) coupled to a single ^{15}N quintet. Complex **11** appeared as a ^{6}Li triplet and ^{15}N quintet. Complexation in the presence of trialkylamines depended on the structure of the amine. Triethylamine failed to convert **10** to **12** even at 5.0 M triethylamine (Et_3N). The less sterically demanding *N*,*N*-dimethylethylamine (DMEA), by contrast, readily afforded amine solvate **12** at >0.30 M DMEA. Elevated concentrations of DMEA converted **12** to LiHMDS monomer **14** and free ketone **1**, as shown with IR and NMR spectroscopies. Of importance to the rate studies was that complex **12** persisted as the dominant form of the ketone at elevated LiHMDS concentrations. Notably, ketone **1** was more easily dissociated than less hindered ketones.[8]

On first inspection, the inclusion of toluene-solvated monomer **13** may seem unusual. However, previous studies of LiHMDS/trialkylamines showed substantial hydrocarbon cosolvent effects.[11] Poor resolution precluded such investigations of DMEA/hydrocarbon mixtures. The results from spectroscopic studies using Et_2NMe/toluene mixtures illustrate qualitatively the magnitude of such toluene effects on the dimer−monomer equilibria (Figure 7).

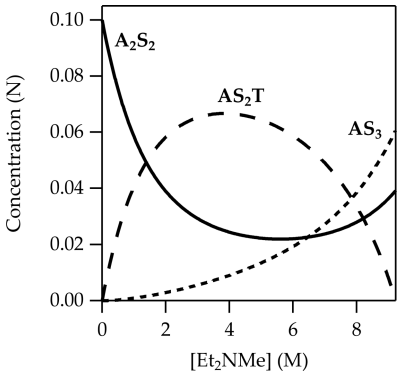

Figure 7. Simulated plot of LiHMDS aggregate concentrations—A_2S_2, AS_2T, and AS_3—as a function of Et_2NMe concentration in toluene highlighting the influence of toluene.[11]

Enolate Structures: DMEA. Enolization of **1** using 1.0 equiv of LiHMDS in DMEA/toluene afforded homoaggregated enolates as broad mounds in the ^{6}Li spectra, which suggested oligomerization (possibly laddering[22]). By contrast, enolization using ≥2.0 equiv of [^{6}Li, ^{15}N]LiHMDS afforded lithium enolate−LiHMDS mixed aggregate[8] ***E*-15** along with traces of ***Z*-15**, consistent with the >100:1 *E*/*Z* selectivity observed with tosylation.[6] The dimeric mixed aggregates displayed characteristic $^{6}Li-^{15}N$ coupling (3.6 Hz) and offered an independent measure of the *E*/*Z* selectivity. Treating the mixed dimers with THF afforded ***E*,*E*-2**, traces of ***E*,*Z*-2**, and free LiHMDS monomer. DFT computations were used to probe the solvation of LiHMDS−enolate mixed aggregates, and the *E*- and *Z*-enolate mixed dimers were shown to be disolvated ***E*-15** and ***Z*-15**, respectively.

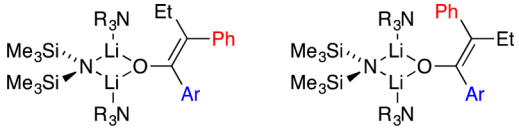

Enolization Mechanism: Et_3N. LiHMDS/Et_3N-mediated enolizations are mechanistically simple and familiar from previous studies.[8] The results of in situ IR spectroscopy showed that enolizations of **1** with LiHMDS in Et_3N/toluene at 0 °C involved first-order decays of complex **10** (1671 cm^{-1}). A kinetic isotope effect (k_H/k_D = 7) confirmed rate-limiting proton transfer. A plot of k_{obsd} versus Et_3N concentration (Figure 8) and *free* LiHMDS concentration (Figure 9) showed first and zeroth orders, respectively. Unsolvated complex **10** was observed spectroscopically. The rate law in eq 8 is consistent with the mechanism described by eqs 9 and 10. Replacing toluene with hexane caused a limited (1.3-fold) rate increase.

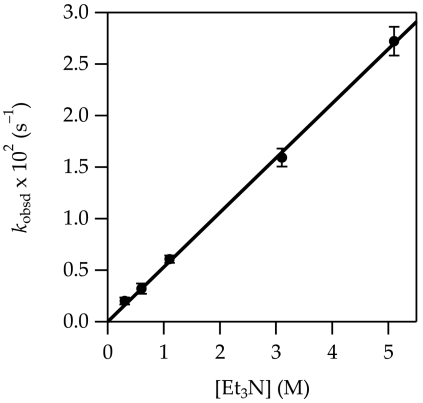

Figure 8. Plot of k_{obsd} vs Et_3N concentration in toluene for the enolization of **1** (0.0050 M) with LiHMDS (0.10 M) at 0 °C measured with IR spectroscopy (1671 cm^{-1}). The curve depicts an unweighted least-squares fit to $y = ax^n$ (a = 0.53 ± 0.03, n = 1.00 ± 0.03). Analogous linearity and reaction order are replicated by the more complex function described in the text.

DOI: 10.1021/jacs.7b05057
J. Am. Chem. Soc. 2017, 139, 12182−12189

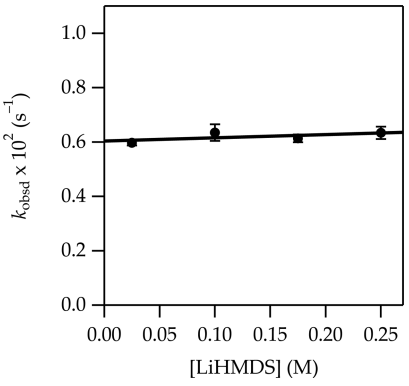

Figure 9. Plot of k_{obsd} vs LiHMDS concentration in 1.10 M Et_3N/toluene for the enolization of **1** (0.0025 M) at 0 °C measured with IR spectroscopy (1671 cm^{-1}). The curve depicts an unweighted least-squares fit to $y = ax + b$ ($a = 0.60 \pm 0.02$, $b = 0.1 \pm 0.1$).

$$d[\mathbf{10}]/dt = k[\mathbf{10}][Et_3N] \quad (8)$$

$$A_2(\text{ketone}) \underset{}{\overset{K_{eq}[Et_3N]}{\rightleftharpoons}} A_2(\text{ketone})(Et_3N) \quad (9)$$
$$\mathbf{10} \qquad\qquad \mathbf{12}$$

$$A_2(\text{ketone})(Et_3N) \xrightarrow{k} [A_2(Et_3N)(\text{ketone})]^{\ddagger} \quad (10)$$
$$\mathbf{12} \qquad\qquad \mathbf{17}$$

DFT computations of the dimer-based metalation probed open dimer-based transition structures (**16**) bearing 8-membered rings that allowed for optimal collinear proton transfer. In all cases, however, the computations converged on closed structures ***E*-17** and ***Z*-17** (eq 11). The relative energies were congruent with those of a highly *E*-selective enolization.

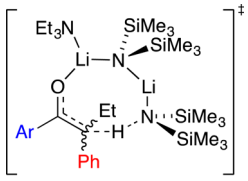

16

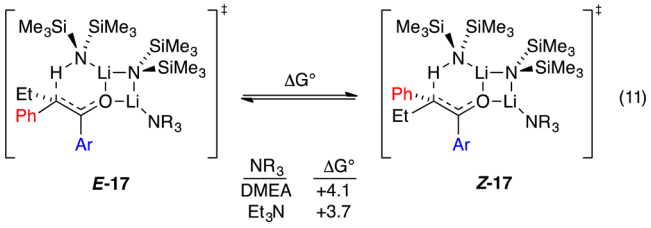

***E*-17** ***Z*-17** (11)

NR_3	ΔG°
DMEA	+4.1
Et_3N	+3.7

Enolization Mechanism: DMEA. Rate studies using DMEA were significantly more challenging owing to condition-dependent solution structures, as shown in Scheme 2. The enolizations of **1** with LiHMDS in 0.60 M DMEA/toluene at −40 °C—conditions favoring solvated complex **12**—showed first-order decays of **12** (1671 cm^{-1}), and the measured isotope effect ($k_H/k_D = 8$) confirmed rate-limiting proton transfer. Plotting k_{obsd} versus DMEA concentration (Figure 10) was complex, but the results were consistent with the observed structural changes: a first-order dependence at the low-DMEA-concentration limit akin to that observed for Et_3N abruptly gave way to inhibition owing to facile decomplexation (*vide infra*). Swapping toluene with hexane as the cosolvent (see Figure 10, inset) revealed an

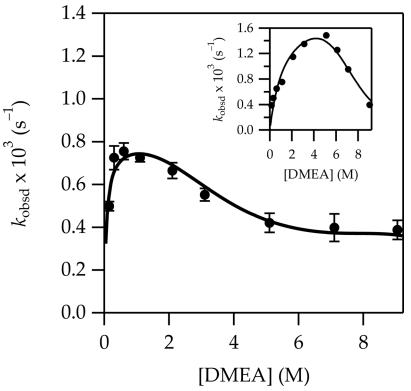

Figure 10. Plot of k_{obsd} vs DMEA concentration with toluene cosolvent for the enolization of **1** (0.0050 M) with LiHMDS (0.10 M) at −40 °C measured with IR spectroscopy (1671 cm^{-1}). The inset shows analogous data for hexane cosolvent. The curves depict unweighted least-squares fits to eq 12, which is described fully in the Supporting Information. Notably, the function describing the dependence of complex **12** in eq 12 changes with the choice of cosolvent.

analogous result but with the maximum shifted to higher DMEA concentrations consistent with the relative stabilization of uncomplexed LiHMDS monomer with toluene versus hexane.

A plot of k_{obsd} versus LiHMDS concentration (Figure 11) at 0.60 M DMEA revealed a zeroth-order dependence consistent

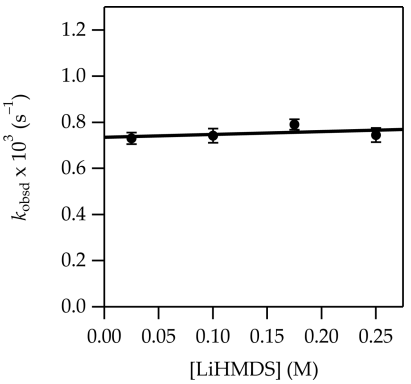

Figure 11. Plot of k_{obsd} vs LiHMDS concentration in 0.60 M DMEA/toluene for the enolization of **1** (0.0025 M) at −40 °C measured with IR spectroscopy (1671 cm^{-1}). The curve depicts an unweighted least-squares fit to $y = ax + b$ ($a = 0.74 \pm 0.02$, $b = 0.12 \pm 0.02$).

with the direct reaction of complex **12**. Thus, the rate law at low DMEA concentration was consistent with that of a monosolvated-dimer-based enolization as observed for Et_3N (eq 9). A plot of k_{obsd} versus LiHMDS concentration in neat DMEA, conditions in which uncomplexed ketone dominated at low LiHMDS concentration and became complexed as dimer **12** at high LiHMDS concentration, showed second-order saturation (Figure 12). This result, in conjunction with the high *E*/*Z* selectivities determined with NMR spectroscopy and high-performance liquid chromatography analysis under these conditions, confirmed that monomer **14** *reaggregated* to complex **12** before reacting. The rate law and mechanism are described by eqs 12−15 below.

Mathematical Model. The rate of enolization is described by eq 12. The challenges of solving for the concentration of **12** were acute because this value is a function of the concentrations of four components (eq 13). The overall equation that describes

DOI: 10.1021/jacs.7b05057
J. Am. Chem. Soc. 2017, 139, 12182−12189

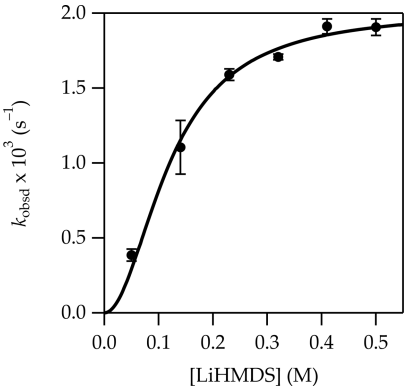

Figure 12. Plot of k_{obsd} vs LiHMDS concentration in neat DMEA (9.2 M) for the enolization of **1** (0.0050 M) at −40 °C measured with IR spectroscopy (1687 cm^{-1}). The curve depicts an unweighted least-squares fit to eq 12, which is described fully in the Supporting Information.

the concentration of **12** is cumbersome (huge) and relegated to the Supporting Information. In brief, the model accounts for the complex curvatures shown in Figure 10. The flattening at high DMEA concentrations is not only demanded by the rate data but also by the known toluene dependence illustrated in Figure 7. The *second*-order (rather than first-order) saturation behavior in Figure 12 could be debated based on the data alone, but it is required by the observable LiHMDS-concentration-dependent reaggregation of monomer **14** to form complexed LiHMDS dimer **12** at the saturation plateau. Finally, the model includes provisions for the simple dependencies in Figures 8, 9, and 11, which call for much simpler functions if one ignores the shifting structures.

$$d[\mathbf{15}]/dt = k'[\mathbf{12}] \quad (12)$$

$$[\mathbf{12}] = f([\text{LiHMDS}], [\mathbf{1}]_{total}, [\text{DMEA}], [\text{toluene}]) \quad (13)$$

$$\underset{\mathbf{12}}{A_2(\text{DMEA})(\mathbf{1})} \xrightarrow{k'} \underset{\textit{E}\text{-}\mathbf{17}}{[A_2(\text{DMEA})(\mathbf{1})]^{\ddagger}} \quad (14)$$

DISCUSSION

Tetrasubstituted alkene moieties as central motifs of GDC-0810 and a number of key anticancer agents pose particularly daunting synthetic challenges.[1−4] The potentially general solution to the problem presented in Scheme 1 is notable, yet the mediocre stereoselectivity obtained using LiHMDS/THF for the enolization of **1** underscores a central challenge. LiHMDS in DMEA/toluene solves the problem of stereoselectivity. Reversing the roles of the Ar and Ph moieties offers the final puzzle piece—full stereo*control*.[5]

Structural and mechanistic studies of the enolizations are summarized in Scheme 1. Enolization with LiHMDS in neat THF affords an ensemble of ***E,E*-2**, ***E,Z*-2**, and ***Z,Z*-2** dimeric enolates that reflect the 1:6 *E*/*Z* selectivity confirmed by the trapping with Ts_2O described in a previous paper.[5] Reduced THF concentrations reverse the selectivity, promoting a slight (2:1) preference for ***E*-2**. The results of rate studies reveal that the *E* selectivity stems from a dominant *tetrasolvated*-monomer-based pathway, whereas the *Z* selectivity arises from a *pentasolvated*-monomer-based pathway. The different selectivities may originate from closed and open transition structures (respectively) or even contact- and solvent-separated ion pairs, but such highly solvated systems defy scrutiny with DFT methods. Attempts to compute transition structures with lower solvation numbers (**18**, n = 1−3) were not predictive and are relegated to the Supporting Information. Structures **18a** and **18b** are merely artists' renditions. We also hasten to add that minor contributions from other solvates could easily go undetected, but the THF-concentration-dependent change in selectivity stems primarily from a differential solvation by only one THF (see Figure 4).

Previous studies showed that LiHMDS in trialkylamine/hydrocarbon mixtures enolize simple ketones (eq 1) with extraordinarily high selectivity via a dimer-based pathway suggested by MNDO computations to be **6**.[8] Indeed, the enolization of **1** with LiHMDS/DMEA or LiHMDS/Et_3N afforded what may be an even more extraordinary 65:1 *E*/*Z* selectivity. The resulting enolates in poorly coordinating trialkylamines form mixed aggregates ***E*-15** and ***Z*-15** in proportions consistent with trapping experiments.[5] Adding THF converted the mixed aggregates to an ensemble of dimers dominated by homodimer ***E,E*-2**.

The results of structural and mechanistic studies using Et_3N show that ketone complex **11** is *not* observably solvated to form **12**. However, rate study findings clearly implicate monosolvated-dimer-based transition structure ***E*-17** analogous to results with

Scheme 3. Summary of Mechanisms for the Enolization of Ketone 1 Using LiHMDS

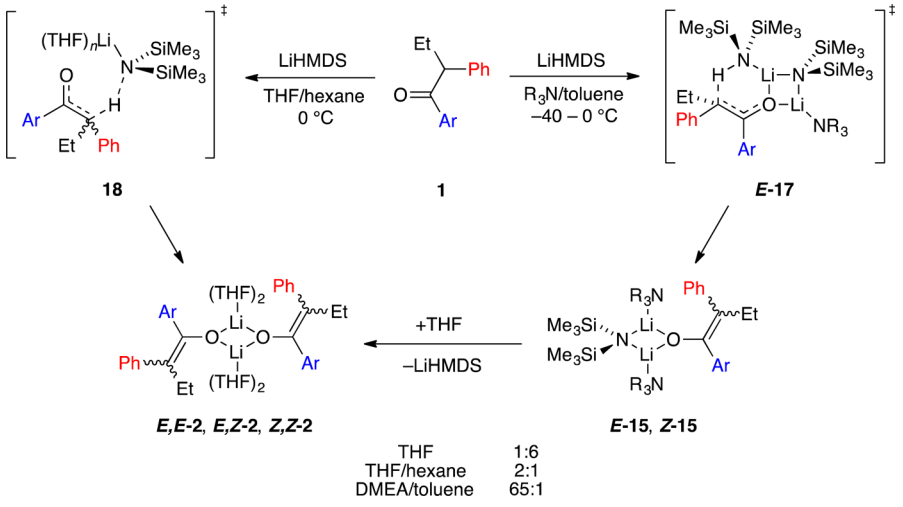

DOI: 10.1021/jacs.7b05057
J. Am. Chem. Soc. 2017, 139, 12182−12189

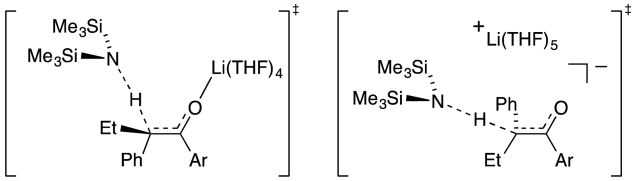

18a 18b

the less congested ketones.[8] The developing mixed dimer motif in ***E*-17**—the developing transannular Li−O contact—was observed computationally to the exclusion of the 8-membered ring depicted in **6**. We reinvestigated **6** with 3-pentanone using DFT and found that the transition structure converged on the closed motif ***E*-19** analogous to ***E*-17**. In all cases, intrinsic reaction coordinate calculations in the reverse direction reveal a lengthening on the transannular Li−O contact toward a structure resembling that of **6**.

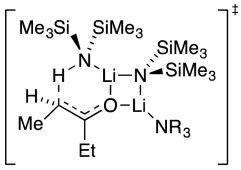

***E*-19**

This summary seems neat and tidy and almost simple, but the structural and mechanistic complexity should not be underestimated. Ketone complex **11** is readily converted to the corresponding solvate **12** at low concentrations of the relatively unhindered DMEA. Elevated DMEA concentrations, however, deaggregate **12** to form LiHMDS monomer with the concomitant liberation of free ketone. Moreover, LiHMDS deaggregation is remarkably sensitive to the choice of hydrocarbon cosolvent, as noted previously for LiHMDS/*N*,*N*-diethylmethylamine.[11] In DMEA/hexane, the sole observable monomer is trisolvate **14**. Toluene, by contrast, stabilizes the monomer and promotes deaggregation and decomplexation owing to the intervention of disolvated monomer **13** stabilized by a molecule of toluene. Whether toluene is explicitly bound is unknown, but the fit to an explicit solvate is excellent.

At this point, the data analysis becomes gruesome. Although parallel pathways from a common ground state are readily deconvoluted, we are just beginning to develop the numerical skills to model systems with multiple condition-dependent reactants.[20] The fit in Figure 10, for example, is based on a complex equation crudely outlined in eqs 12−14 and described thoroughly in the Supporting Information. The slight upward curvature at the high DMEA concentrations in Figure 10 stems from contributions by the toluene-solvated monomer. The model includes provisions for simple dependencies in the other figures as well.

We highlight a key observation about the role of aggregate-based reactivity for LiHMDS/DMEA. In neat DMEA, the dominant form of LiHMDS is trisolvated LiHMDS monomer **14** uncomplexed by ketone; however, highly *E*-selective enolization and saturation kinetics (see Figure 12) show that the preferred pathway involves *reaggregation* to complexed dimer **12** (observable at the saturation plateau) and enolization via dimer-based transition structure ***E*-17**. The notion that a monomer would *reaggregate* to react seems blasphemous, but evidence supporting such processes has begun to accumulate (including a LiHMDS/THF-mediated enolization).[12b,20,23]

CONCLUSION

The preceding analyses presented a particularly interesting problem in which a pharmaceutical need for an acutely challenging stereoselective enolization aligned with an academic interest in solvation and aggregation effects on enolizations. The application of LiHMDS/trialkylamine mixtures to enolizations has been largely (although not entirely) of academic interest until now.[8] LiHMDS in trialkylamine−hydrocarbon mixtures is a highly efficacious, cost-effective base−solvent combination.

The notion that stereoselectivity stems from (at least) two discrete pathways is a truism with implications that can be overlooked. The idea that selectivity can be controlled by diverting a monomer-based enolization to a dimer-based pathway or by merely decreasing the solvation number by a single solvent is more nuanced. To this end, we emphasize that it is not only constructive to vary solvents during optimizations but also to vary solvent *concentration*s and even the hydrocarbon cosolvent.[12a]

EXPERIMENTAL SECTION

Reagents and Solvents. THF, toluene, hexane, and the trialkylamines were distilled from blue or purple solutions containing sodium benzophenone ketyl. LiHMDS, [^{6}Li]LiHMDS, and [^{6}Li, ^{15}N]LiHMDS were prepared as ligand- and LiCl-free recrystallized solids.[9] Ketone **1** was prepared as described in a preceding paper.[5] Air- and moisture-sensitive materials were manipulated under argon using standard glovebox, vacuum line, and syringe techniques.

2-Deutero-1-(4-fluorophenyl)-2-phenylbutan-1-one (1-d_1). Following a literature procedure,[24] we charged a small vial with 1.0 g of **1** in 2.5 mL of MeOD under positive argon flow. To the vial was added 1.0 mL of 2.60 M NaOD/D_2O. The solution was stirred for 30 min. The vial was opened, and 35% DCl was added until the solution was neutralized. Three extractions were performed with pentane, followed by solvent removal in vacuo. The oil was further purified via column chromatography (10% ether/pentane) to afford 0.86 g of **1-d_1** (86% yield) as a clear, slightly yellow oil. The results of ^{1}H NMR spectroscopy and gas chromatography−mass spectroscopy showed >99% **1-d_1**.

IR Spectroscopic Analyses. IR spectra were recorded using an in situ IR spectrometer fitted with a 30-bounce, silicon-tipped probe. The spectra were acquired in 16 scans at a gain of 1 and a resolution of 4 cm^{-1}. A representative reaction was carried out as follows: The IR probe was inserted through a nylon adapter and O-ring seal into an oven-dried, cylindrical flask fitted with a magnetic stir bar and a T-joint. The T-joint was capped with a septum for injections and a nitrogen line. After evacuation under full vacuum, heating, and flushing with nitrogen, the flask was charged with LiHMDS (84 mg, 0.50 mmol) in THF/hexane (4.9 mL total volume) and cooled to 0 °C with a stirred ice bath. After recording a background spectrum, we added ketone **1** (0.050 mmol in 0.10 mL) with stirring. The carbonyl absorbance at 1687 cm^{-1} was monitored over the course of the reaction.

NMR Spectroscopic Analyses. All NMR samples for reaction monitoring and structure elucidation were prepared using stock solutions and sealed under partial vacuum. Standard ^{1}H, ^{6}Li, ^{13}C, and ^{15}N NMR spectra were recorded at 500, 73.57, 125.79, and 36.14 MHz, respectively.

ASSOCIATED CONTENT

Supporting Information

The Supporting Information is available free of charge on the ACS Publications website at DOI: 10.1021/jacs.7b05057.

Spectroscopic, kinetic, and computational data and complete ref 13 (PDF)

AUTHOR INFORMATION

Corresponding Author

*dbc6@cornell.edu

DOI: 10.1021/jacs.7b05057
J. Am. Chem. Soc. 2017, 139, 12182−12189

ORCID
Haiming Zhang: 0000-0002-2139-2598
Francis Gosselin: 0000-0001-9812-4180
David B. Collum: 0000-0001-6065-1655

Notes

The authors declare no competing financial interest.

■ ACKNOWLEDGMENTS

In memory of Dr. Andrew McClory who tragically passed away on February 19, 2017. D.B.C. and K.A.M. thank the National Institutes of Health (GM077167 and GM039764) for financial support and the National Science Foundation (NSF-MRI, CHE-1531632) for support of the Cornell NMR facility.

■ REFERENCES

(1) Lai, A.; Kahraman, M.; Govek, S.; Nagasawa, J.; Bonnefous, C.; Julien, J.; Douglas, K.; Sensintaffar, J.; Lu, N.; Lee, K.-j; Aparicio, A.; Kaufman, J.; Qian, J.; Shao, G.; Prudente, R.; Moon, M. J.; Joseph, J. D.; Darimont, B.; Brigham, D.; Grillot, K.; Heyman, R.; Rix, P. J.; Hager, J. H.; Smith, N. D. *J. Med. Chem.* **2015**, *58*, 4888.

(2) (a) DeGregorio, M. W.; Wiebe, V. J. *Tamoxifen and Breast Cancer*, 2nd ed.; Yale University Press: New Haven, CT, 1999. (b) Levenson, A. S.; Jordan, V. C. *Eur. J. Cancer* **1999**, *35*, 1628.

(3) McCague, R.; Leclercq, G.; Legros, N.; Goodman, J.; Blackburn, G. M.; Jarman, M.; Foster, A. B. *J. Med. Chem.* **1989**, *32*, 2527.

(4) Connor, C. E.; Norris, J. D.; Broadwater, G.; Willson, T. M.; Gottardis, M. M.; Dewhirst, M. W.; McDonnell, D. P. *Cancer Res.* **2001**, *61*, 2917.

(5) Li, B. X.; Le, D. N.; Mack, K. A.; McClory, A.; Lim, N.-K.; Cravillion, T.; Savage, S.; Han, C.; Collum, D. B.; Zhang, H.; Gosselin, F. *J. Am. Chem. Soc.* **2017**, *139*, 10777.

(6) Early examples of *E*/*Z* enolization selectivities: (a) Masamune, S.; Ellingboe, J. W.; Choy, W. *J. Am. Chem. Soc.* **1982**, *104*, 5526. (b) Gaudemar, M.; Bellassoued, M. *Tetrahedron Lett.* **1989**, *30*, 2779. (c) Heathcock, C. H.; Buse, C. T.; Kleschick, W. A.; Pirrung, M. C.; Sohn, J. E.; Lampe, J. *J. Org. Chem.* **1980**, *45*, 1066. (d) McCarthy, P. A.; Kageyama, M. *J. Org. Chem.* **1987**, *52*, 4681. (j) Davis, F. A.; Sheppard, A. C.; Chen, B.-C.; Haque, M. S. *J. Am. Chem. Soc.* **1990**, *112*, 6679.

(7) Zhao, P.; Condo, A.; Keresztes, I.; Collum, D. B. *J. Am. Chem. Soc.* **2004**, *126*, 3113.

(8) (a) Godenschwager, P.; Collum, D. B. *J. Am. Chem. Soc.* **2008**, *130*, 8726. (b) Zhao, P.; Collum, D. B. *J. Am. Chem. Soc.* **2003**, *125*, 14411. (c) Snaddon, T. N.; Buchgraber, P.; Schulthoff, S.; Wirtz, C.; Mynott, R.; Furstner, A. *Chem. - Eur. J.* **2010**, *16*, 12133.

(9) (a) Tomasevich, L. L.; Collum, D. B. *J. Am. Chem. Soc.* **2014**, *136*, 9710. (b) Romesberg, F. E.; Bernstein, M. P.; Gilchrist, J. H.; Harrison, A. T.; Fuller, D. J.; Collum, D. B. *J. Am. Chem. Soc.* **1993**, *115*, 3475.

(10) Lucht, B. L.; Collum, D. B. *J. Am. Chem. Soc.* **1995**, *117*, 9863.

(11) Lucht, B. L.; Collum, D. B. *J. Am. Chem. Soc.* **1996**, *118*, 2217.

(12) (a) Collum, D. B.; McNeil, A. J.; Ramírez, A. *Angew. Chem., Int. Ed.* **2007**, *46*, 3002. (b) Algera, R. F.; Gupta, L.; Hoepker, A. C.; Liang, J.; Ma, Y.; Singh, K. J.; Collum, D. B. *J. Org. Chem.* **2017**, *82*, 4513.

(13) Frisch, M. J.; Trucks, G. W.; Schlegel, H. B.; Scuseria, G. E.; Robb, M. A.; Cheeseman, J. R.; Montgomery, J. A., Jr.; Vreven, T.; Kudin, K. N.; Burant, J. C.; Millam, J. M.; Iyengar, S. S.; Tomasi, J.; Barone, V.; Mennucci, B.; Cossi, M.; Scalmani, G.; Rega, N.; Petersson, G. A.; Nakatsuji, H.; Hada, M.; Ehara, M.; Toyota, K.; Fukuda, R.; Hasegawa, J.; Ishida, M.; Nakajima, T.; Honda, Y.; Kitao, O.; Nakai, H.; Klene, M.; Li, X.; Knox, J. E.; Hratchian, H. P.; Cross, J. B.; Bakken, V.; Adamo, C.; Jaramillo, J.; Gomperts, R.; Stratmann, R. E.; Yazyev, O.; Austin, A. J.; Cammi, R.; Pomelli, C.; Ochterski, J. W.; Ayala, P. Y.; Morokuma, K.; Voth, G. A.; Salvador, P.; Dannenberg, J. J.; Zakrzewski, V. G.; Dapprich, S.; Daniels, A. D.; Strain, M. C.; Farkas, O.; Malick, D. K.; Rabuck, A. D.; Raghavachari, K.; Foresman, J. B.; Ortiz, J. V.; Cui, Q.; Baboul, A. G.; Clifford, S.; Cioslowski, J.; Stefanov, B. B.; Liu, G.; Liashenko, A.; Piskorz, P.; Komaromi, I.; Martin, R. L.; Fox, D. J.; Keith, T.; Al-Laham, M. A.; Peng, C. Y.; Nanayakkara, A.; Challacombe, M.; Gill, P. M. W.; Johnson, B.; Chen, W.; Wong, M. W.; Gonzalez, C.; Pople, J. A. *Gaussian 3.09*, revision B.04; Gaussian, Inc.: Wallingford, CT, 2009.

(14) (a) Renny, J. S.; Tomasevich, L. L.; Tallmadge, E. H.; Collum, D. B. *Angew. Chem., Int. Ed.* **2013**, *52*, 11998. (b) Liou, L. R.; McNeil, A. J.; Ramírez, A.; Toombes, G. E. S.; Gruver, J. M.; Collum, D. B. *J. Am. Chem. Soc.* **2008**, *130*, 4859.

(15) Measuring the mole fraction within only the ensemble of interest rather than the overall mole fraction of lithium alkoxides added to the samples eliminates the distorting effects of impurities.

(16) Job, P. *Ann. Chim.* **1928**, *9*, 113.

(17) Legault, C. Y. *CYLview*, 1.0b; Université de Sherbrooke: 2009 (http://www.cylview.org).

(18) Rein, A. J.; Donahue, S. M.; Pavlosky, M. A. *Curr. Opin. Drug Discovery Dev.* **2000**, *3*, 734.

(19) Casado, J.; Lopez-Quintela, M. A.; Lorenzo-Barral, F. M. *J. Chem. Educ.* **1986**, *63*, 450.

(20) Reyes-Rodríguez, G. J.; Algera, R. F.; Collum, D. B. *J. Am. Chem. Soc.* **2017**, *139*, 1233.

(21) The rate law provides the stoichiometry of the transition structure relative to that of the reactants: Edwards, J. O.; Greene, E. F.; Ross, J. *J. Chem. Educ.* **1968**, *45*, 381.

(22) (a) Gregory, K.; Schleyer, P. v. R.; Snaith, R. *Adv. Inorg. Chem.* **1991**, *37*, 47. (b) Mulvey, R. E. *Chem. Soc. Rev.* **1991**, *20*, 167.

(23) (a) Lucht, B. L.; Bernstein, M. P.; Remenar, J. F.; Collum, D. B. *J. Am. Chem. Soc.* **1996**, *118*, 10707. (b) Liang, J.; Hoepker, A. C.; Algera, R. F.; Ma, Y.; Collum, D. B. *J. Am. Chem. Soc.* **2015**, *137*, 6292. (c) Plessel, K. N.; Jones, A. C.; Wherritt, D. J.; Maksymowicz, R. M.; Poweleit, E. T.; Reich, H. J. *Org. Lett.* **2015**, *17*, 2310.

(24) Tomioka, H.; Hayashi, N.; Izawa, Y.; Senthilnathan, V. P.; Platz, M. S. *J. Am. Chem. Soc.* **1983**, *105*, 5053.

DOI: 10.1021/jacs.7b05057
J. Am. Chem. Soc. 2017, 139, 12182−12189